

Distribution of subcritical Hopf bifurcations and regular and chaotic attractors in optical bistable systems

Hu Gang,* Cun-zheng Ning, and H. Haken

*Institut für Theoretische Physik und Synergetik, Universität Stuttgart, Pfaffenwaldring 57/4,
D-7000 Stuttgart 80, Federal Republic of Germany*

(Received 3 August 1989)

The distributions, in parameter space, of subcritical Hopf bifurcations and the various attractors of time-dependent motions of optical bistable systems are investigated systematically. The main emphasis is placed on the influence of the variations of the control parameters on the distributions. We have observed the tristability of large-amplitude regular or chaotic motions, periodic pulsations, and the stationary state for the parameters where no instability of the stationary solution exists at all over the complete range of the external field. The problem of how to find the various attractors and how to reveal chaotic motions by adjusting the control parameters is discussed according to the numerical results.

I. INTRODUCTION

Since the first observation of optical bistability¹ (OB), the study of OB systems has become one of the most active fields in nonlinear optics.²⁻⁵ In recent decades, much attention has been attracted by the instabilities and chaotic motions manifested in the OB systems.⁵⁻¹⁵ The interest is due to both practical and theoretical reasons. Practically, it is of crucial importance to understand the instabilities and various erratic motions of OB in order to design optical bistable devices possessing required functions. Theoretically, the OB systems are used as a good example to show the rich characteristic behaviors of nonlinear dynamic systems.

In this paper we focus on a simplified OB system which contains an optical unidirectional ring cavity filled with a passive medium, consisting of homogeneously broadened two-level atoms, and driven by an external coherent optical signal. We consider only the single-mode case. With the plane-wave approximation, and the mean-field limit,¹² we can reduce the Maxwell-Bloch equations to

$$\begin{aligned} \frac{dx}{dt} &= -k[(1+i\theta)x - y + 2Cp], \\ \frac{dp}{dt} &= xD - (1+i\Delta)p, \\ \frac{dD}{dt} &= -\gamma[(x^*p + xp^*)/2 + D - 1], \end{aligned} \quad (1.1)$$

where x and p are the normalized slowly varying complex output field and the atomic polarization, respectively. D is the normalized real population difference of the two-level atoms. The parameter C is the bistability parameter and γ and k are the longitudinal decay rate and the cavity linewidth, respectively, scaled by the transverse relaxation rate γ_{\perp} . The frequencies of the external field, the cavity, and the atoms are denoted by ω_0 , ω_c , and ω_a , respectively. The two detuning parameters are defined as

$$\theta = (\omega_c - \omega_0)/(k\gamma_{\perp}),$$

$$\Delta = (\omega_a - \omega_0)/\gamma_{\perp}.$$

The normalized amplitude of the external field y is assumed to be real and positive.

Equations (1.1) possess the stationary solution

$$\begin{aligned} y &= |x_s| \{ [1 + 2C/(1 + \Delta^2 + |x_s|^2)]^2 \\ &\quad + [\theta - 2C\Delta/(1 + \Delta^2 + |x_s|^2)]^2 \}^{1/2}, \\ D_s &= (1 + \Delta^2)/(1 + \Delta^2 + |x_s|^2), \\ p_s &= (1 - i\Delta)x_s/(1 + \Delta + |x_s|^2). \end{aligned} \quad (1.2)$$

As C is larger than some critical value, which depends on Δ and θ and is equal to 4 as $\Delta = \theta = 0$, the solution curve on the y - $|x_s|$ plane is S shaped. The negative-slope part of the stationary solution curve is unstable. Thus one may obtain bistability for the given parameters.

The model specified by Eqs. (1.1) was first derived and formulated by Bonifacio and Lugiato.¹⁶ Since then these equations have been extensively studied in a number of publications. On the one hand, they are simple enough, for instance, in comparison with hydrodynamic systems, to allow systematic theoretical investigation. On the other hand, it is interesting enough to show many kinds of complexity of nonlinear dynamic systems, and relatively realistic to permit a comparison with experimental results in certain important circumstances. For example, Eqs. (1.1) predict absorptive as well as dispersive bistability as C exceeds a certain critical value (as we stated previously). That can be used to clarify the mechanism of the experimental observation of optical bistability. In fact, by studying Eqs. (1.1), Lugiato, Narducci, and co-workers obtained the instability boundary in the control parameter space that is qualitatively and semiquantitatively in agreement with the experimental observations.^{14,17,18}

It has been shown that as the bistability parameter C is large enough, the oscillation arising from the instability of the stationary solution may undergo further period-doubling bifurcations and result in chaos. However, experiments have not yet confirmed the existence of chaotic motion predicted by (1.1) while the parameter values in experiments are well within the required domain. Lugiato and Narducci imputed the apparent discrepancy to the invalidity of the plane-wave approximation.^{17,18} It has been shown that by incorporating a Gaussian transverse electric field the period-doubling bifurcations as well as chaos arising in Eqs. (1.1) can be ruled out, and the theoretical results are in good agreement with the experimental observations.^{13,17,18} It is, then, expected¹⁸ that the more complicated as well as interesting behaviors including various higher-order bifurcations and chaos predicted by (1.1) may be realized by improving the experimental setting, therefore better fulfilling the uniform-field condition in the transverse direction.

But, as a matter of fact, Eqs. (1.1) are far from being fully understood. Actually, they have been investigated in detail only in various limiting cases and in a few sets of selected parameters. A number of problems of substantial importance remain to be answered. One of them is the structure of attracting basins of (1.1). Which attractors does the system approach when the positive-slope stationary solution loses its stability? Furthermore, are there any attractors as the positive-slope solution remains stable? Which kinds of attractors are they if there are? How are these unknown attractors affected by adjusting the control parameters? The answer to these questions

will, of course, shed new light on the understanding of the global structure of the dynamics of the OB systems.

In Refs. 19 and 20, together with Yang, one of us (Hu) has analyzed the instability regions of (1.1) in detail, and provided an intuitive picture about the distribution of the instability regions in the control parameter space. In Ref. 21, we specified the condition for super- and subcritical Hopf bifurcations. For a few concrete combinations of parameters we have distinguished sub- and supercritical bifurcations and plotted some new related attractors.

This paper is an essential continuation of Ref. 21. We will focus on the global distribution of subcritical bifurcation and the distribution of the attractors of time-dependent motion and study how to modify the attractors and to find higher-order temporal structures and chaotic motion by adjusting the control parameters. In the latter part of this section we will briefly review the general formulations presented in Refs. 19 and 21. In the central part of the presentation, Secs. II–IV, we will present numerical results, based on the analytic achievements in Refs. 19 and 21. In Sec. II distribution of the instability boundary and the subcritical bifurcation on the boundary will be clearly shown. In Sec. III we exhibit three kinds of attractors and reveal how the domains of the existence of the attractors can be modified by changing the control parameters. In Sec. V we focus on chaotic motion and try to discuss the problem in which parameter regions chaos may probably be found in the OB systems. Section VI will give some brief discussions.

About the stationary solution (1.2), Eqs. (1.1) can be linearized as

$$\frac{d}{dt} \begin{pmatrix} \delta x \\ \delta x^* \\ \delta p \\ \delta p^* \\ \delta D \end{pmatrix} = \begin{pmatrix} -k(1+i\theta) & 0 & -2Ck & 0 & 0 \\ 0 & -k(1-i\theta) & 0 & -2Ck & 0 \\ D & 0 & -(1+i\Delta) & 0 & x_s \\ 0 & D & 0 & -(1-i\Delta) & x_s \\ -rp_s^*/2 & -rp_s/2 & -rx_s^*/2 & -rx_s/2 & -r \end{pmatrix} \begin{pmatrix} \delta x \\ \delta x^* \\ \delta p \\ \delta p^* \\ \delta D \end{pmatrix}, \tag{1.3}$$

where

$$\delta x = x - x_s, \quad \delta p = p - p_s, \quad \delta D = D - D_s.$$

The corresponding eigenvalue equation is given by

$$\lambda^5 + a_1\lambda^4 + a_2\lambda^3 + a_3\lambda^2 + a_4\lambda + a_5 = 0. \tag{1.4}$$

In the following we will simply use X instead of $|x_s|$. All the coefficients in (1.4) can be expressed in terms of the external control parameters $C, \gamma, k, \Delta, \theta$, and X . The concrete forms of $a_1 \rightarrow a_5$ are explicitly given in Refs. 19 and 21. In Ref. 19, an analytic function

$$f = (a_1 a_2 - a_3)(a_3 a_4 - a_2 a_5) - (a_1 a_4 - a_5)^2 \tag{1.5}$$

was defined. It has been proved that, starting from a stable region, the necessary and sufficient condition for the instability of the stationary solution is that one of the following two surfaces

$$a_5 = 0, \tag{1.6a}$$

$$f = 0 \tag{1.6b}$$

is crossed transversely, for the first time (the two critical surfaces will be called surface A and B respectively; for an exact definition, see Ref. 21). Based on (1.6) the instability boundary of OB can be predicted systematically in the control parameter space.

The Hopf bifurcation may be supercritical or subcritical. different types of bifurcations may lead to substantially different behaviors. To distinguish them, the linearized equations (1.3) are not sufficient. One should take into account both linear and nonlinear terms in Eqs. (1.1). At the Hopf bifurcation point the normal form of Eqs. (1.1) can be written as²²

$$\begin{aligned} r &= \bar{G}_3 r^3 + \bar{G}_5 r^5 + \dots, \\ \phi &= \Omega + O(r^2), \end{aligned} \tag{1.7}$$

where ϕ is the phase angle, r is the radial coordinate, and Ω is the characteristic frequency at the bifurcation point. In Ref. 21, applying the slaving principle,^{23,24} we reduced the five-dimensional Eqs. (1.1) to two-dimensional order-parameter equations and gave an analytic form of G_3 in terms of the control parameters. We do not intend to use much space to write down the concrete forms of $a_1 \rightarrow a_5$ and G_3 (G_3 refers to the \bar{G}_3 at the exact critical point) explicitly. Instead, we directly use them in our numerical simulations and refer the readers to Refs. 19 and 21 for the exact formulas. It is obvious that in the case of

$$G_3 > 0 \quad (1.8)$$

the Hopf bifurcation is subcritical, and that in the opposite case

$$G_3 < 0 \quad (1.9)$$

the bifurcation is supercritical. A small-amplitude limit cycle arises for the case of (1.9) while an oscillation with finite amplitude might arise in the case of (1.8).

II. DISTRIBUTION OF INSTABILITY REGIONS AND SUB- AND SUPERCRITICAL BIFURCATIONS

A. Instability regions of OB

In this section, we will first present several figures of the instability regions. In Ref. 20, the Hopf unstable region on the x axis was lacking which is very important for distinguishing sub- and supercritical bifurcations and for studying various attractors. Hence, we will give some results about this matter in this section.

In Fig. 1, we fix $C=200$, $\theta=-10$, $k=0.5$, $\gamma=1$, and have Δ and X varied. The dotted line indicates surface A , while the solid line surface B . At the intersections of both surfaces we have codimension-2 bifurcations of type IIIB (see Ref. 21) at which the linear part of the normal form of Eqs. (1.1) reads

$$\begin{pmatrix} 0 & \Omega & 0 \\ -\Omega & 0 & 0 \\ 0 & 0 & 0 \end{pmatrix}$$

(see Ref. 22). Henceforth we will denote the instability region surrounded by boundary A the N region (negative-slope region) and that by boundary B the H region (Hopf instability region). Both regions contain closed areas. In Fig. 1 the N area is not closed. However, it would be closed as we consider smaller Δ , which we are not interested in because no Hopf instability exists there. The numbers 1–4 mark the four intersections of A and B ; each one can be distinguished from the others according to the topological structure of the intersections of two closed curves. [The simplest way to recognize each intersection is the following: 1, the intersection of the right boundary of the N region with the upper boundary of the H region; 2, that of the left N region and the upper H region; 3, that of the left N region and the lower H (or the left H) region; 4, the right N region and the lower H region.] In the part of the H region left (right) to

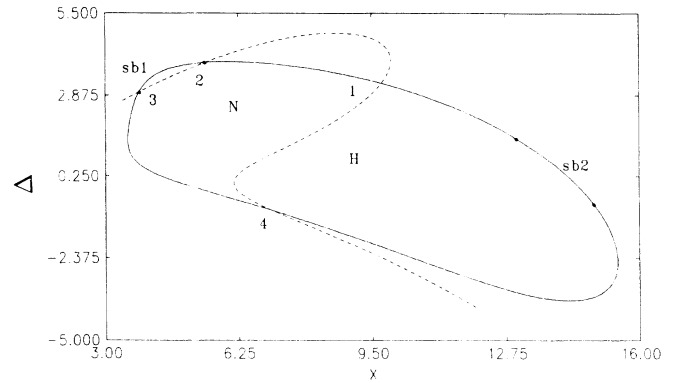


FIG. 1. Instability regions and subcritical segments of OB. The parameter values are $C=200$, $k=0.5$, $\gamma=1$, and $\theta=-10$. In region N surrounded by the dashed line, the stationary solution curve has negative slope and is unstable. In region H surrounded by the solid curve, the stationary solution is destabilized by the Hopf bifurcation. In segments sb1 and sb2 the Hopf bifurcation is subcritical, while it is supercritical on the remained positive-slope instability boundary. The dashed and solid curves have four intersections marked 1–4, respectively.

the N region, a segment of the lower (the upper) branch of the stationary solution is destabilized by Hopf bifurcation. Above the N region, no S-shaped solution exists. The stationary solution is single valued there.

An interesting problem is how the H region can be modified by changing the control parameters. In Figs. 2(a)–2(d), we provide a series of plots for varied parameters. From all the figures it is noticed that the H region is always a single closed area. It can be expanded or contracted, even contracted to nothing, by altering the control parameters.

By decreasing the decay rate of the atomic population difference γ the lower boundary of the H region may be shifted up, and the H area is contracted. Moreover, the whole H region may be pushed to the direction of larger X . Thus, first intersections 2 and 3 and then those of 1 and 4 disappear successively by continuously reducing γ . (Remember, the N region is not affected by changing either γ or k .) In Fig. 2(a), we take $\gamma=0.05$ and have all the other parameters unvaried from Fig. 1. The H area is apparently much smaller than that in Fig. 1 and no intersection of A and B exists at all. It is worth noting that a completely isolated region, i.e., a positive-slope instability island, occurs in Fig. 2(a). Increasing γ , we may find things to be just the opposite.

The influence of varying k on the H region is clearly exposed in Figs. 2(b) and 2(c). In Fig. 2(b), the other parameters are the same as in Fig. 1 while k is decreased to 0.1. The upper boundary of the H region may withdraw considerably. That is just in contrast with what happens by decreasing γ . Now the whole H area is contracted as in Fig. 2(a). The intersections of A and B disappear in the same way as that of decreasing γ . As k is increased, the upper boundary of the H region shifts to the direction of larger X , and the whole H region expands. Intersections 1 and 2 may get closer, merge, and finally disappear because the upper boundary of H goes up. The above

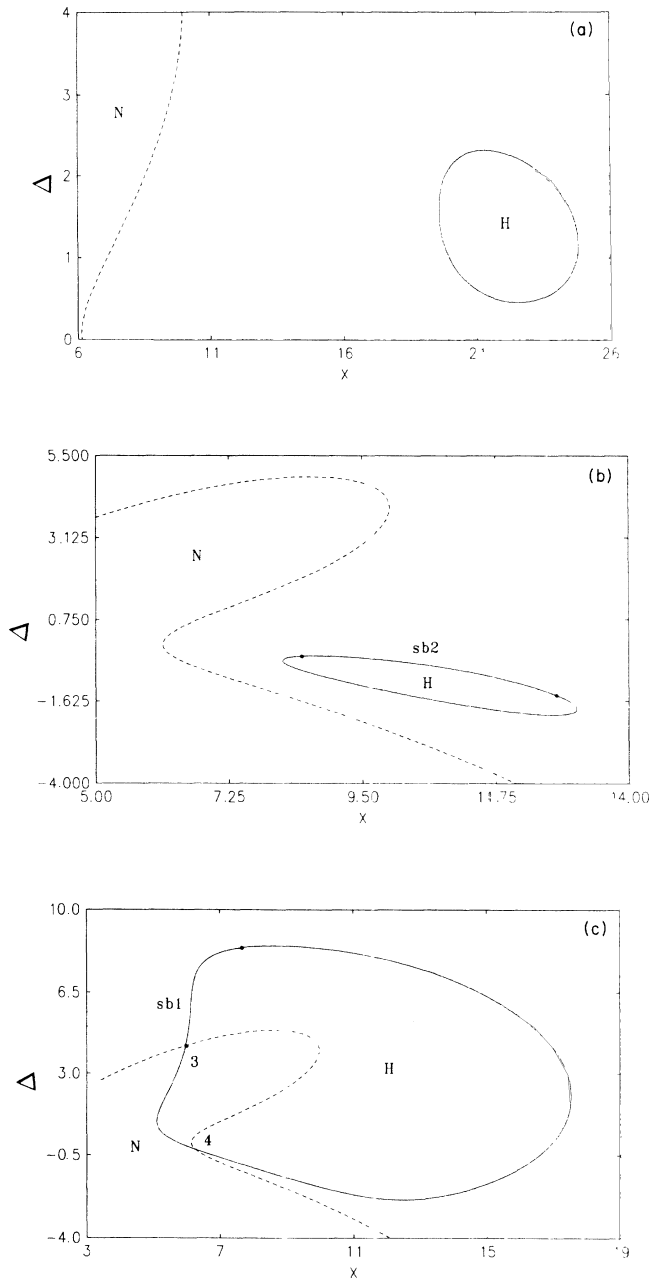


FIG. 2. (a) The parameter values are the same as in Fig. 1 except that γ is reduced to $\gamma=0.05$. The H region is considerably contracted, and the intersection of the dashed and the solid lines disappears because the H region is pushed to the right. On the entire boundary of the H region the Hopf bifurcation is supercritical. (b) $k=0.1$; and all the other parameters are given in Fig. 1. The Hopf instability region is very much contracted, compared with that in Fig. 1. The subcritical bifurcation segment sb2 covers a major portion of the upper instability boundary of the H region. (c) $k=1$; the other parameters are given in Fig. 1. The Hopf instability region is enlarged. Intersections 1 and 2 disappear because the upper boundary of the H region is up. In contrast to (b), now sb2 disappears while sb1 enlarges. (d) $C=75$; the other parameters are given in Fig. 1. The H region is considerably contracted. Segments sb2 are reduced to nothing.

phenomena can be seen in Fig. 2(c) where we take $k=1$. By further increasing k , the H region is pushed to the right and up; intersections 3 and 4 disappear eventually at large k .

Both the N and H regions can be altered by varying C . In Fig. 2(d), we reduce C to $C=75$, and maintain the other parameters unchanged from Fig. 1. Intersections 1 and 2 disappear because the N region is pushed down and left. The H region is considerably contracted in comparison with that in Fig. 1. As C is further reduced, intersections 3 and 4 disappear and even the entire N and H regions themselves will eventually vanish for very small C .

In the previous statements we take some space to describe the presence of the codimension-2 bifurcation set (the intersections of curves A and B) because it has been found, numerically, that this set has some relation with the subcritical Hopf bifurcation of Eqs. (1.1). This fact will be described in Sec. II B.

To display the influence of varying θ on the H and N regions, it is better to consider the bifurcation phase diagram in the $X-\theta$ plane. In Figs. 3(a)–3(c), we take C , γ , and k to be the same as in Fig. 1, and fix $\Delta=0$, 1.5, and 4, respectively. In Fig. 3(a) both the N and H regions are symmetrical with respect to the x axis. In contrast with the figure on the $X-\Delta$ plane, now the H region contains two unclosed parts. In Fig. 3(b), the symmetry is broken by a nonzero Δ . Then, the H region in the half plane $\Delta\theta>0$ becomes a closed region. Meanwhile in the other half plane $\Delta\theta<0$, the H region is still open and its area enlarges as Δ increases. Increasing Δ , we may more and more reduce the area of the H region in the half plane $\Delta\theta>0$. Finally, this domain vanishes for relatively large Δ . In Fig. 3(c), at $\Delta=4$, we can no longer find the H region in the upper half of the $X-\theta$ plane.

B. Subcritical bifurcation of OB

Having specified the instability boundary B , we may be able to distinguish subcritical and supercritical bifurcation by calculating G_3 . The concrete form of G_3 was given in Ref. 21. The calculation leads to the results shown in Figs. 1–3. In all the segments sb1 and sb2, the Hopf bifurcation is subcritical. It is supercritical otherwise (of course, only the positive-slope Hopf instability needs to be taken into account). In respect to the distribution of subcritical Hopf bifurcation, the following comments can be made from the figures.

(i) Whenever intersection 3 appears we always find a subcritical bifurcation segment immediately following the intersection. This segment is denoted by sb1 in Figs. 1–3. sb1 covers almost the entire left part of the positive-slope instability boundary. Therefore, in most cases the Hopf instability of the lower branch is subcritical. This observation is in good agreement with Ref. 15, where it was found that for large C the Hopf bifurcation in the lower branch is subcritical. sb1 may persist even as intersection 3 disappears. sb1 always vanishes after the disappearance of intersection 3.

(ii) On the lower boundary of the H region in the $X-\Delta$

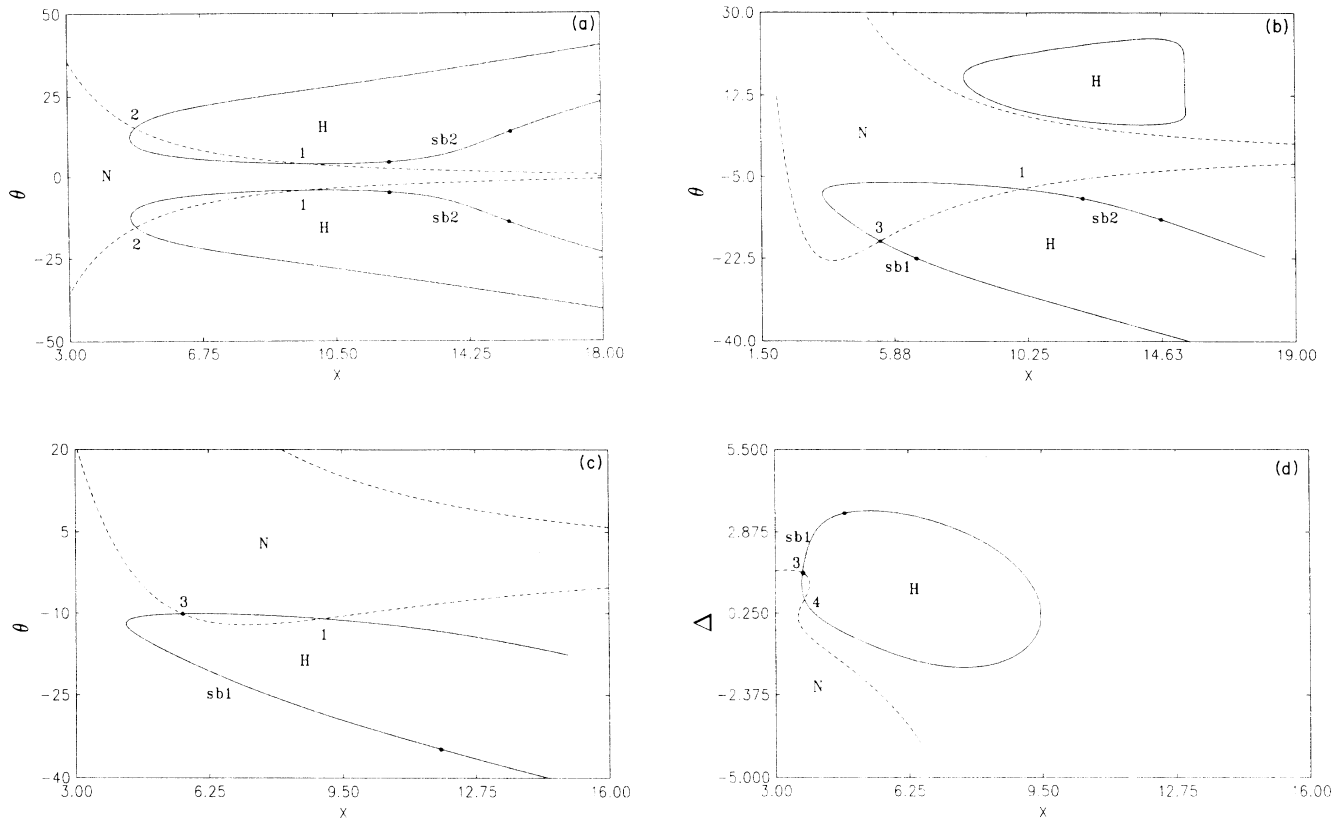


FIG. 3. (a) The instability region in the X - θ plane. C , k , and γ are given in Fig. 1. $\Delta=0$. There are two H regions located symmetrically with respect to the x axis. Only the sb2 subcritical bifurcation segment is found. (b) Δ is raised to 1.5; all the other parameters are the same as in (a). Now the H region in the upper half plane becomes a closed area. Subcritical bifurcation does not exist in this half plane. In the lower half plane, the length of segment sb2 is reduced and segment sb1 appears. (c) $\Delta=4$. The other parameters remain unchanged from (a). The H region no longer exists in the upper half plane. In the lower half plane, segment sb2 disappears while that of sb1 considerably enlarges.

plane the positive-slope Hopf bifurcation is always supercritical. This means that the Hopf bifurcation on the upper branch of the S-shaped curve must be supercritical if the bifurcation arises on the side of the H region with smaller $|\Delta|$. This observation is partially in agreement with the findings in Ref. 15.

(iii) On the upper boundary of the H region there may exist a subcritical bifurcation island between supercritical bifurcation segments that is denoted by sb2. Thus, on the upper boundary of the H region, the Hopf bifurcation in the upper branch of the stationary solution may be supercritical or subcritical according to the particular combination of the parameters. This conclusion is a complement of the statement in Ref. 15.

(iv) For the Hopf instability domain in the X - θ plane, larger $|\Delta|$ always favors sb1, while relatively smaller $|\Delta|$ favors sb2. This fact is exhibited more clearly in Fig. 3. Moreover, in the Y - X plane, the subcritical bifurcation on the border of smaller X of the unstable segment belongs to sb1, while that on the border of larger X belongs to sb2.

The subcritical bifurcation segments can be varied by changing the control parameters. The change is partially shown in Figs. 1–3.

Decreasing C or γ , we may reduce the sizes of both sb1

and sb2, and eventually rule out the subcritical bifurcation segments. For instance, in Fig. 2(a) ($\gamma=0.05$), only a supercritical bifurcation exists on the entire positive-slope bifurcation boundary. In Fig. 2(d), as C is decreased to $C=75$, sb2 disappears. We have observed that at $C=30$ with k , γ , and θ being given in Fig. 1, the H region still exists (though its area is considerably reduced) while the Hopf bifurcation is purely supercritical; neither sb1 (as well as intersection 3) nor sb2 remains.

The influence of changing k on the subcritical bifurcation segments is worthwhile noting. It seems that increasing k favors sb1 while decreasing k favors sb2. In Fig. 2(b), at $k=0.1$ the H region has been contracted to a very small area and the segment sb1 completely disappears. However, the subcritical segment sb2 grows to cover the major portion of the upper boundary of the H region. On the contrary, in Fig. 2(c) sb2 disappears and sb1 considerably enlarges at $k=1$.

From Fig. 3 where sb1 and sb2 have the same meaning as in Figs. 1 and 2, one may get an impression of how the subcritical bifurcation segments are affected by changing Δ and θ . It is observed that at small enough $|\Delta|$ [in Fig. 2(a)] sb1 does not exist. As $|\Delta|$ increases, sb2 contracts, while sb1 occurs and enlarges in the half plane $\Delta\theta < 0$. (One can never find sb1 in the part $\Delta\theta > 0$.) For large

enough $|\Delta|$ [for instance, in Fig. 3(c) we have $\Delta=4$] sb2 disappears completely; the subcritical bifurcation completely belongs to sb1. It is also noted from Fig. 3 that, given Δ , the Hopf bifurcation is definitely supercritical for a very large $|\theta|$.

In the above discussion we specified subcritical bifurcation by sb1 and sb2. On the one hand, they are indeed distinguished from each other by the location in the parameter space as well as the variable space as stated in (i), (iii), and (iv). On the other hand, this distinction leads to an essential consequence in the dynamics of the system. It will be found in Sec. III that, after the instability of sb2, the system may be led to an attractor different from that of sb1.

With Figs. 1–3 and the related comments in mind, we already have a clear picture of the global structure of the instability regions of OB and the distribution of the subcritical bifurcation segments on the instability boundary. We may be able to control the instability regions or to reveal subcritical Hopf bifurcation segments by adjusting various parameters. It should be emphasized that the preceding comments have been verified not only for the particular sets of parameters taken in Figs. 1–3, but also for a wide range of parameter domains. In fact, we have varied C from 10 to 10^3 , γ from 10^{-2} to 2, k from 10^{-2} to 10, and Δ and θ from 0 to tens that covers almost the entire physically interesting domain of OB, and all observations coincide with our statements. Moreover, the distribution of the instability regions and the classification of subcritical and supercritical bifurcations are also justified by directly integrating Eqs. (1.1).

III. ATTRACTORS OF TIME-DEPENDENT MOTION

After the specification of the distribution of the instability regions and the classification of supercritical and subcritical bifurcations, further problems naturally arise: Which attractors does the system approach after the instability of its stationary solution, and are there any other attractors even if the stationary solution is entirely stable? The central task in this section is to reveal the existence of new attractors of time-dependent motion and to find out how these attractors can be modified by adjusting the control parameters.

A. Three attractors of time-dependent motion

First we present Fig. 4 to give an intuitive picture about the attractors. In Fig. 4, we take $C=200$, $\theta=-20$, $\Delta=7$, $\gamma=2$, and $k=0.5$. To draw the curves in the figure, we numerically solve Eqs. (1.1) for a given Y and a set of the initial variables x_i , p_i , and D_i , for long enough time to ensure that the evolution is well after the transient process, and then plot the X which is maximal in a final time interval that is much larger than the characteristic period [for instance, $2\pi/\Omega$ with Ω being given in Eq. (1.7)]. The curves are plotted by taking possible Y and the initial variables. The curves so plotted will be called M curves afterwards. It is obvious that each M curve represents an independent attractor.

After a careful searching in a wide region in the variable space by taking possible combinations of x_i , p_i , and

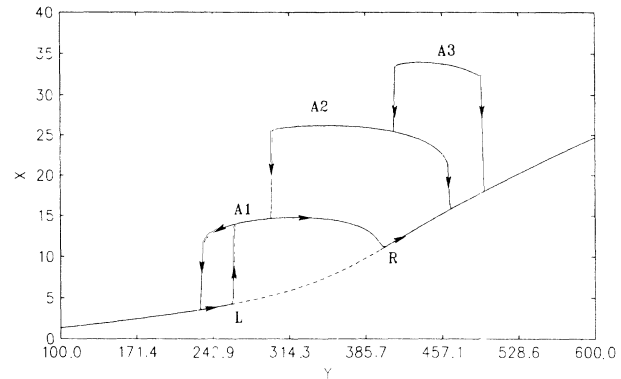


FIG. 4. M curve in the X - Y plane. $C=200$, $k=0.5$, $r=2$, $\theta=-20$, and $\Delta=7$. After the transient process of Eqs. (1.1), the maximum X in the trajectory is plotted against Y . Different M curves indicate different attractors. We mark the three attractors, apart from the attractor of the stationary solution, as A1, A2, and A3, in the order of increasing heights of the M curves.

D_i , we obtain four M curves in Fig. 4. The lowest curve represents the stationary solution in which the dashed curve LR indicates the unstable segment that, of course, cannot be found in the above manner. For the parameters given in Fig. 4 no S-shaped segment exists. The instability is purely due to Hopf bifurcation. At point L , the lower boundary of the unstable segment, the Hopf bifurcation is subcritical (in fact, L is exactly on the sb1 region), while at R , the upper boundary, it is supercritical. The arrows on the curves denote the possible direction on which the system may go by continuously varying the external field Y . It is a great surprise that one may find three attractors apart from that of the stationary solution. In Fig. 4 we denote the three by A1, A2, and A3, respectively. [$H(A3) > H(A2) > H(A1)$, $H(A_j)$ is the height of the curve A_j .] It seems that the attractor A1 has a closer relationship with the stationary solution. It can be reached by starting from the stable stationary solution and adjusting the external field continuously from both sides of the Hopf instability boundaries. From the lower side, the system jumps discontinuously to A1 immediately after the subcritical bifurcation point L is exceeded. From the upper side, the system goes into A1 continuously by reducing Y lower than Y_R . On the contrary, the basins of A2 and A3 are far away from the stationary solution. One cannot feel the presence of A2 and A3, starting from a stationary solution and continuously varying Y . To reach A2 or A3, one should carefully choose certain initial values of the variables. When we have reached A2 or A3, we may stay there by continuously varying Y till the border of the M curves is reached. Over the border, the system will jump down either to the lower M curve or to the stable stationary solution.

An interesting point is that, though the stationary solution curve is not S shaped at the present parameters, there exists a bistability between the stable stationary solution and the periodic solution A1 in Fig. 4.

The sizes of the M curves may be modified by changing the control parameters. In Figs. 5(a)–5(e), we take different combinations of the parameters. In Fig. 5(a), we

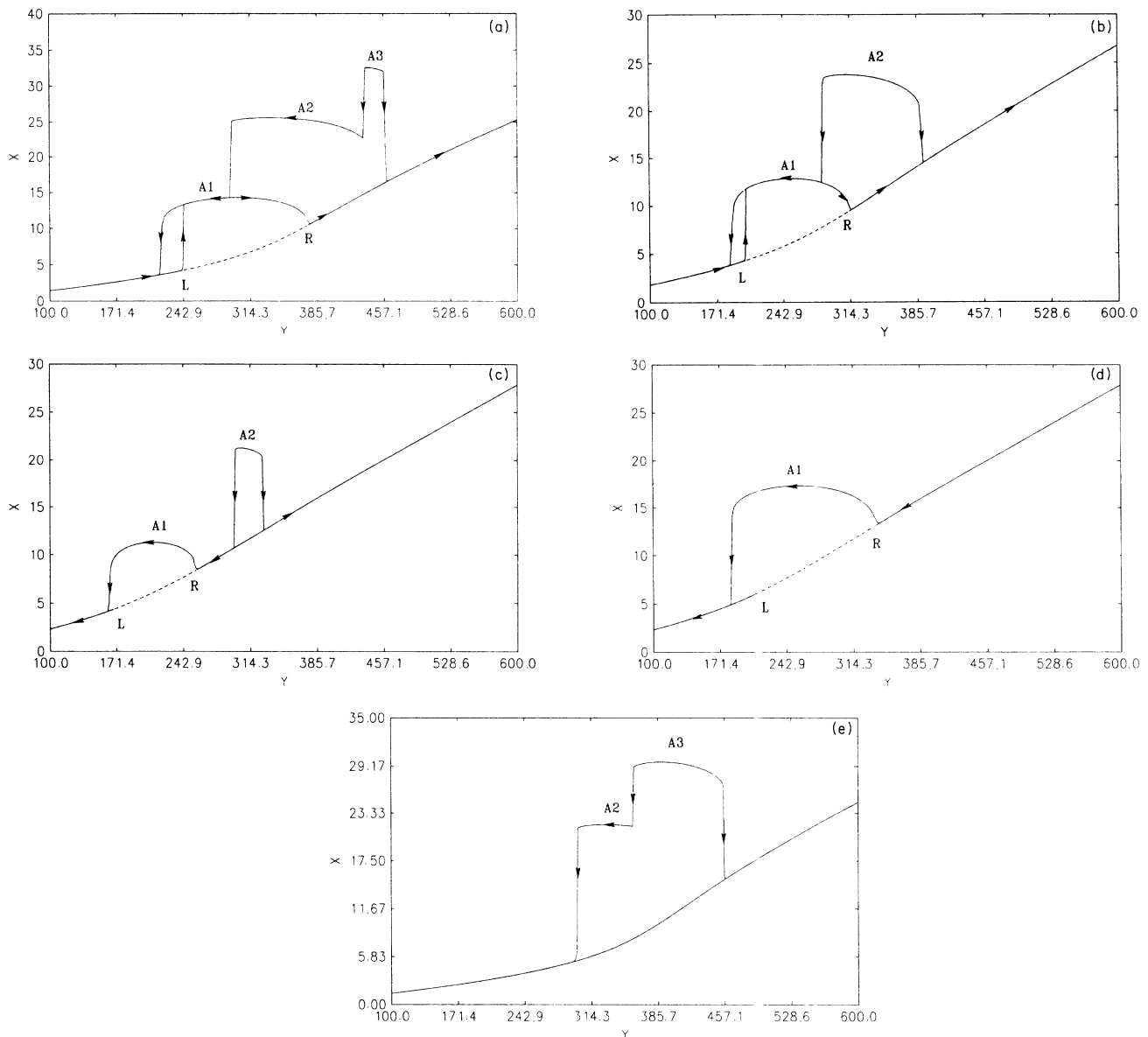


FIG. 5. (a) $C = 180$; the other parameters are the same as in Fig. 4. The M curve $A3$ is considerably shortened. (b) C is reduced to 130; the other parameters are given in Fig. 4. $A3$ completely disappears. (c) C is further reduced to 90; the other parameters remain unchanged from Fig. 4. $A1$ and $A2$ are much reduced and separated from each other. (d) $k = 0.7$; all the other parameters are the same as in (c). $A2$ completely disappears. (e) $k = 0.4$; all the other parameters are kept the same as in Fig. 4. No instability of the stationary solution occurs, and consequently, the M curve $A1$ disappears. On the contrary, $A2$ and $A3$ exist, and even the length of the curve $A3$ enlarges in comparison with that of Fig. 4.

lower the bistability parameter C to $C = 180$, and the size of the M curve $A3$ becomes much smaller. In Fig. 5(b) C is reduced to $C = 130$, and $A3$ completely disappears. As we further decrease C to $C = 90$, both $A1$ and $A2$ are contracted and they are separated from each other on the y axis. In Fig. 5(d), we increase k to 0.7 while keeping all other parameters the same as in Fig. 5(c); $A2$ eventually disappears, while the size of $A1$ enlarges.

Nevertheless, one should not be led to the impression that the attractors of oscillation with larger amplitude always disappear earlier than those with smaller amplitude. In Fig. 5(e) we take all parameters the same as in Fig. 1

but $k = 0.4$. It is found that the entire stationary solution is stable; there is neither Hopf bifurcation nor the M curve $A1$. However, the attractors $A2$ and $A3$ do exist, and even the size of $A3$ enlarges. Therefore, we would like to emphasize a striking property of the system; namely, a stable pulsation can exist in the system (1.1) even if no instability of the stationary solution occurs.

There are seemingly some regularities on modifying the various attractors by varying the control parameters. With much experience of the numerical solution of the system, we are led to the following conclusions.

(i) The attractor $A1$ is closely related to the Hopf insta-

bility of the stationary solution. By controlling the positive-slope instability segment one may roughly control the size of A1.

(ii) Decreasing (increasing) the bistability parameter C , one may reduce (enlarge) the size of each M curve of time-dependent motion. For small enough C , all the M curves other than the stationary solution curve may eventually disappear. (We have found A2 at $C=75$, and A1 as well as the Hopf instability of the stationary solution at $C=12$, which is much lower than the known threshold for the Hopf bifurcation to take place.)

(iii) Decreasing γ may definitely reduce the sizes of all A1, A2, and A3, and eventually make them disappear at sufficiently small γ .

(iv) The influence on the M curves by changing k is more delicate. It seems that for a given set of C , γ , Δ , and θ , increasing k favors the attractor A1 while decreasing k favors the asymptotic oscillation with larger amplitude. This fact is found in Figs. 5(d) and 5(e), and is justified by several integrations for other parameters.

(v) A definite statement for the influence on A2 and A3 of changing Δ and θ is difficult. Nevertheless, it is found that, for given Δ , C , γ , and k , A2 and A3 can be made smaller and then disappear by sufficiently increasing or decreasing $|\theta|$. A2 and A3 can be found only on the middle range of θ . Given C , k , γ , and θ , a similar behavior can also be observed for changing Δ .

B. Relationships between attractors

In Figs. 4 and 5, both the subcritical bifurcation at L and the supercritical bifurcation at R lead to an oscillation in A1. The other attractors seem not to be related to the stationary solution. This situation can be essentially changed in several ways.

(i) The bifurcation on the upper boundary may become subcritical (on the segment sb2 in Figs. 1–3). In this case, the system often jumps directly to a large-amplitude oscillation from the stationary state. In Fig. 6, the sys-

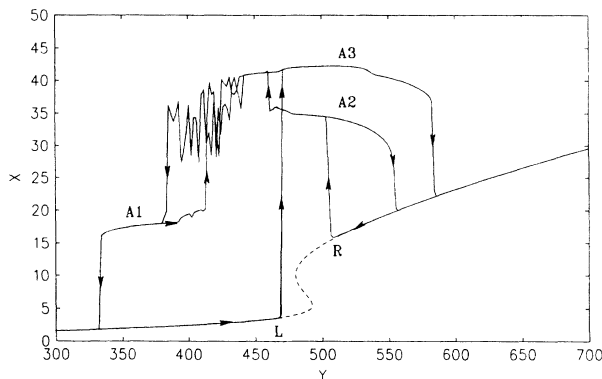


FIG. 6. $C=400$, $k=0.4$, $\gamma=1.76$, $\Delta=-4$, and $\theta=20$. The Hopf bifurcation at the upper branch R is subcritical. The system jumps from the stationary solution to A2 after Y is slightly lower than Y_R . Moreover, certain segments of both A1 and A2 are unstable, and the system may jump up from A1 and A2 to A3. Increasing Y slightly over Y_L , the system can jump from the lower branch of the stationary solution to A2 and A3, according to the initial conditions.

tem jumps from the upper branch directly to the attractor A2 immediately after Y is reduced over R . This observation has been justified by all our numerical results for $C > 100$. Thus, as the Hopf bifurcation at the upper border R becomes subcritical, one may be able to reach the attractors A2 or A3 by starting from the stable stationary state and continuously decreasing the external force Y .

(ii) The time-dependent states on the various attractors may undergo further instability, and then the system may jump not only from upper M curves to lower ones, as what happens in Figs. 4 and 5, but also from lower to upper. The latter case can be found in Fig. 6 where it is shown that the system is able to jump from A1 to A3 as a segment of A1 turns to be unstable and can also jump from A2 to A3 before jumping down to the lower attractors. In Fig. 6, the system can even jump from the lower branch of the stationary solution directly to A2 or A3 as L is exceeded. This happens in the case where A1 is already unstable for the given Y . In all those cases, one may again be able to reach the attractors of larger-amplitude oscillation from the stationary solution by continuously varying the control parameters. The question of whether a state of time-dependent solution can be reached by continuously varying the control parameters from the stationary state or not is of importance because in experiments one usually realizes the pulsation in this way. Figure 6 is typical because it gathers various transitions between various attractors in a single diagram. Those transitions can also be found, but, in general, only separately, in other figures.

To conclude this section we would like to remark upon the hysteresis structure of the time-dependent asymptotic motions. In Fig. 6, we can easily identify three hysteresis loops. The bistability, or rather, multistability structure of the OB systems is much more complicated than what has been known before, as the time-dependent asymptotic motions are taken into account.

In most of the numerical solutions we observe three or less attractors of time-dependent motion. The coexistence of more attractors cannot be excluded. In fact, we have found the coexistence of four time-dependent motions. Nevertheless, this phenomenon is seldom observed.

IV. PERIOD-DOUBLING BIFURCATIONS AND CHAOS

Revealing and clarifying chaotic motion is one of the interesting tasks in displaying the rich nonlinear dynamic behaviors in the OB systems. Nevertheless, to date, chaotic motion in OB has been found only occasionally. It is not clear how chaotic motions can be found or controlled by adjusting the control parameters. In this paper, we do not intend to analyze in detail the various characteristic features of chaotic motion or the fine bifurcation sequences leading to chaos. We only try to give a suggestion, based on the numerical observations, as to where chaotic motion can more probably be found and how its existence is affected by changing the control parameters. Our suggestion may be of help in numerically or, possibly, experimentally searching for chaos.

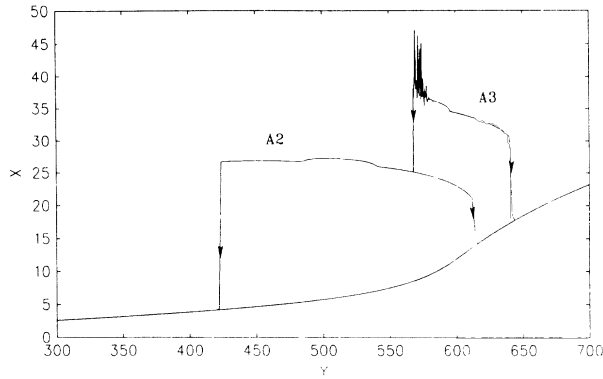


FIG. 7. $\Delta = -7.5$; all the other parameters are given in Fig. 6. No instability of the stationary solution arises. However, chaos can be found in the segment of A3 where the M curve behaves erratically.

After C exceeds 300 (or even lower), the routes to chaos via period-doubling bifurcations as well as intermittency can be observed. In Figs. 4 and 5 the M curves are smooth. Correspondingly, the asymptotic solution is found to be stationary or periodic with the basic period. The same behavior is verified in all the curves in Figs. 6–9 when the M curves are smooth. Whenever certain discontinuity, for instance, the discontinuity of the first derivative of the M curve occurs, one always finds that the motion undergoes a characteristic change, e.g., period doubling. In the segments where the M curve varies violently, one can find chaotic motion. In fact, we numerically observe the route to chaos via period-doubling bifurcations for parameters corresponding to the segment of A3 in Fig. 7 where the M curve behaves erratically. At $Y = 580$, the motion of the system is chaotic. The chaotic motion is justified not only by the aperiodic trajectory in the phase space but also by the positive Lyapunov exponent of Eqs. (1.1) for the given parameters.

There seems to be a regularity in finding parameter regions where chaotic motion can be observed. For relatively large $|\Delta|$ chaos often first appears near the lower

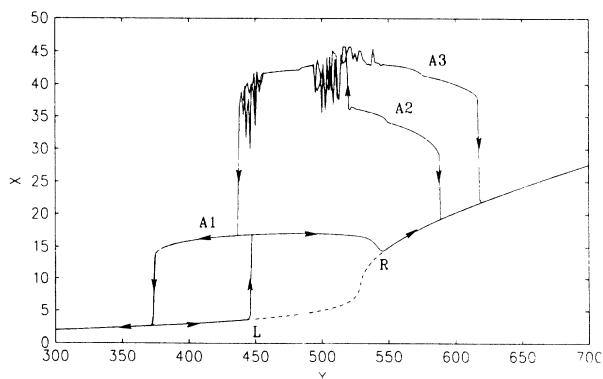


FIG. 8. $\Delta = -5.2$; the other parameters are kept the same as in Fig. 6. Chaos occurs on A3 which cannot be reached by continuously varying the external field Y , starting from the stationary state.

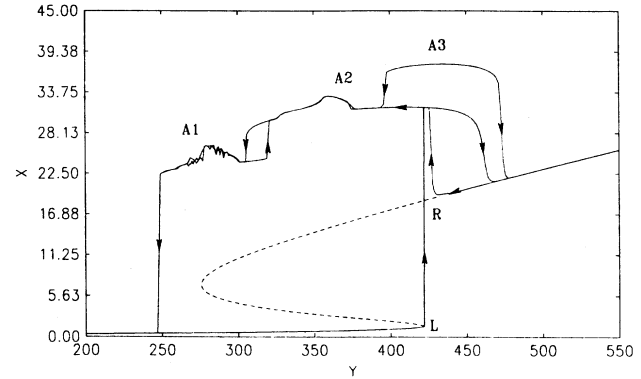


FIG. 9. $\Delta = -1$; the other parameters are given in Fig. 6. For this small $|\Delta|$, chaos can be observed in the lower M curve (A1). A hysteresis loop between A1 and A2 occurs. Period-doubling bifurcations can be observed on both M curves A1 and A2.

boundary of the M curve A3, as indicated in Figs. 6–8. As $|\Delta|$ decreases, the chaotic region may appear in other lower M curves (see Fig. 9).

In Fig. 9, we take the parameter values which have been used in Ref. 17 where a period-doubling bifurcation sequence leading to chaos was reported. The predicted motions are verified in our case. We would like to stress that there is more complicated bifurcation structure around the given parameter region. In fact, on both M curves A1 and A2, period-doubling bifurcations can be observed. The entire bifurcation structure in this multi-basin system is similar to that in Ref. 25 (see Fig. 4 there), where a laser system with an injected signal (LIS) was studied. An important difference between the OB and the LIS is that we have not yet found quasiperiodicity in the OB that was found indeed in the LIS.

Usually, the way one proceeds to detect chaotic motion is the following. First one finds an instability of the stationary state, and then one searches for chaotic motion in the unstable parameter regions. This way is not always successful.

By our detection, chaotic motion extensively exists in the system (1.1) for relatively large (still realizable) C . But in most of cases, it cannot be revealed in the above way. For instance, in Fig. 7 the entire stationary solution is stable, and it can be destabilized neither by Hopf bifurcation nor by saddle-node bifurcation. However, chaotic motion does exist if one takes a suitable Y and starts away from the corresponding stationary solution. Moreover, even if the positive-slope instability occurs, it is still possible that one cannot find chaos by continuously adjusting the external fields from a stable stationary state even though chaotic motion exists for the given parameters. This is the case in Fig. 8. Only under the parameter conditions stated in Sec. III B, can the attractors where chaotic motion takes place be reached from the stationary state by continuously varying the control parameters. This situation is displayed in Figs. 6 and 9.

The awareness that periodic pulsation and chaotic motion may exist in the absence of the instability of the stationary solution in OB is one of the interesting discoveries of the present paper. A similar fact, as an in-

teresting point, has been revealed for the laser Lorenz model.²⁶

V. DISCUSSIONS

Based on the specification of instability regions and classification of subcritical and supercritical bifurcations, we have succeeded in finding, in a systematical way, three attractors of time-dependent motion of the OB systems described in Eqs. (1.1), and possible chaotic motion on the attractors. There is a crucial problem to compare the theoretical finding with experimental results. It was reported¹⁷ that no chaotic motion has been observed in the parameter values where a theoretical study of Eqs. (1.1) predicts chaos. In regard to this matter, we make the following remarks.

(i) In order to observe chaotic motion and the other related complex behaviors, predicted by (1.1), it is necessary to realize experimental settings fulfilling the approximations used in (1.1). Especially, the uniform-field condition in the transverse direction seems to be important in this aspect, as Ref. 18 suggested.

(ii) For the present experimental condition, the reason for the difficulty in finding chaos in experiments may be due to two possible reasons: either no chaotic motion exists at all in the presently realized pure OB systems, or the chaotic region cannot be reached from the stationary state by continuously adjusting the control parameters, as

we argued in Sec. IV. In the latter case, instead of continuously varying parameters, one should design certain mechanisms (for instance, a quick switch of the external field, or a sudden impact of pump, and so on) to push the system far away from the basin of the stationary solution. It might open up a new way of studying the interesting structure of attractors and the possible chaotic motions on the attractors in the OB systems.

(iii) All the behavior found in the presentation can be changed if one takes into account some more realistic systems, for instance, the system with Gaussian transverse field, which has been shown to meet the experimental data better than Eqs. (1.1).^{17,18} Nevertheless, we believe that some characteristic features of (1.1) will be kept in the modified systems. It is interesting to extend the present study to those more realistic and more complex systems. In that study, the understanding of the ideal model (1.1) will be helpful.

Another remarkable point is that the attracting basins of coexisting attractors may be very complicated. It happens that a slight change in the initial variables may lead the system from one attractor to another. For instance, in Fig. 6, the system may jump to A2 or A3, according to fine differences of order 10^{-3} in the initial values of the variables. It is interesting to investigate the attracting domains of the various attractors to study the relation between the onset of chaos with the fractal boundary of the attracting basins in the OB systems. It will be our future work.

*Permanent address: Physics Department, Beijing Normal University, Beijing, People's Republic of China.

¹M. Gibbs, S. L. McCall, and T. N. C. Venkatesan, *Phys. Rev. Lett.* **36**, 1135 (1976).

²R. Bonifacio and P. Meystre, *Opt. Commun.* **29**, 131 (1979).

³E. Abraham and S. D. Smith, *Rep. Prog. Phys.* **45**, 815 (1982).

⁴V. Molonny, H. M. Gibbs, and F. A. Hopf, in *Proceedings of the Topical Meeting on Optical Bistability, Rochester, New York, 1983*, edited by C. M. Bowden, H. M. Gibbs, and S. L. McCall (Plenum, New York, 1984).

⁵H. M. Gibbs, *Optical Bistability: Controlling Light with Light* (Academic, New York, 1985).

⁶V. Benza and L. A. Lugiato, *Lett. Nuovo Cimento* **26**, 405 (1979).

⁷F. A. Hopf, P. Meystre, P. D. Drummond, and D. F. Walls, *Opt. Commun.* **31**, 245 (1979).

⁸K. Ikeda, H. Daido, and O. Akomoto, *Phys. Rev. Lett.* **45**, 709 (1980).

⁹K. Ikeda and O. Akomoto, *Phys. Rev. Lett.* **48**, 617 (1982).

¹⁰L. A. Lugiato, L. M. Narducci, D. K. Bandy, and C. A. Penzance, *Opt. Commun.* **43**, 281 (1982).

¹¹P. D. Drummond, *Opt. Commun.* **40**, 224 (1982).

¹²L. A. Lugiato, in *Progress in Optics*, edited by E. Wolf (North-Holland, Amsterdam, 1984), Vol. XXI.

¹³L. A. Lugiato, R. J. Horowicz, and G. Strini, *Phys. Rev. A* **30**,

1366 (1984).

¹⁴L. A. Lugiato and L. M. Narducci, *Phys. Rev. A* **32**, 1576 (1985).

¹⁵T. Erneux and P. Mandel, *Phys. Rev. A* **33**, 1777 (1986).

¹⁶R. Bonifacio and L. A. Lugiato, *Opt. Commun.* **19**, 172 (1976).

¹⁷L. A. Orozco, H. J. Kimble, A. T. Rosenberger, L. A. Lugiato, M. L. Asquini, M. Brambilla, and L. M. Narducci, *Phys. Rev. A* **39**, 1235 (1989).

¹⁸L. A. Lugiato and L. M. Narducci, *Synergetics and Dynamic Instabilities*, edited by G. Caglioti, H. Haken, and L. A. Lugiato (North-Holland, Amsterdam, 1988).

¹⁹G. Hu and G. J. Yang, *Phys. Rev. A* **38**, 1979 (1988).

²⁰G. J. Yang and G. Hu, *Phys. Rev. A* **39**, 2514 (1989).

²¹G. Hu, C. Z. Ning, and H. Haken, *Phys. Rev. A* **41**, 2702 (1990).

²²J. Guckenheimer and P. Holmes, *Nonlinear Oscillations, Dynamical Systems, and Bifurcations of Vector Fields* (Springer-Verlag, New York, 1983), pp. 352–412.

²³H. Haken, *Synergetics, An Introduction*, 3rd ed. (Springer, New York, 1983).

²⁴H. Haken, *Advanced Synergetics* (Springer, New York, 1983).

²⁵Y. Gu, D. K. Bandy, J. M. Yuan, and L. M. Narducci, *Phys. Rev. A* **31**, 354 (1985).

²⁶L. M. Narducci, H. Sadiky, L. A. Lugiato, and N. B. Abraham, *Opt. Commun.* **55**, 370 (1985).